
Article:
Zhou, L., Brunskill, H. and Lewis, R. orcid.org/0000-0002-4300-0540 (2019) Real-time non-invasive measurement and monitoring of wheel-rail contact using ultrasonic reflectometry. Structural Health Monitoring, 18 (5-6). pp. 1953-1965. ISSN 1475-9217

https://doi.org/10.1177/1475921719829882

Real-Time Non-Invasive Measurement and Monitoring of Wheel-Rail Contact Using Ultrasonic Reflectometry

L. Zhou[1)*], H.P. Brunskill[1)], R. Lewis[1)]

[1)] Department of Mechanical Engineering, University of Sheffield, Sheffield, United Kingdom

*Corresponding author, Email: zhoul540@gmail.com

Abstract

Rail stress levels are vital to the lifespan of rail tracks, and responsible for the safe operation and ride comfort of train services. In particular, wheel-rail contact stress is a dominating factor affecting wear, cracking, fatigue and failure of both wheel and rail. The wheel-rail interaction problem has long been investigated, yet detailed contact information on real cases remains obscure due to the interface complexity, including the varying wheel and rail profiles and lack of effective stress characterisation methods.

Ultrasound image study, as an excellent non-destructive evaluation (NDE) method, is widely used in railway systems for defect detection, stress determination and rail profile checking. Specifically, ultrasonic reflectometry has proved successful in making static machine-element contact measurements. This paper introduces a novel measuring method for both short-term and long-term dynamic wheel-rail contact monitoring purposes based on ultrasonic reflectometry. The method is investigated in detail including the study of ultrasound propagation pathways in the rail, and the optimum placement of ultrasonic elements as well as actuator-receiver combinations. The proposed monitoring technique is expected to characterize and monitor contact behaviour of operating high-speed rail system in real-time.

Key words: Wheel-rail contact, ultrasound, rail condition monitoring, contact stress

1. Introduction

Railway tracks suffer from more and more severe wear, fatigue and health condition problems due to increasing train speeds and loads led by the fast development of the High-Speed Railway (HSR). Regular inspection is necessary in checking for wear and other defects, for maintenance purposes such as necessary regrinding and replacement. For common defect detection in a railway system, various non-destructive evaluation (NDE) methods have been applied including eddy currents [1], optical fibres [2], electromagnetic acoustic transducers (EMATs) [3] and ultrasonic guided waves (UGWs) [4-6]. Most of these are ultrasound-based techniques and railhead checking makes up the majority of rail inspection

tasks. However, wheel-rail contact forces and stresses, which contribute the most to railhead defects, especially rolling contact fatigue (RCF) and subsequent rail surface and sub-surface cracks, currently lack effective characterisation methods.

The contact problem has been studied using Hertz Theory proposed more than a hundred years ago [7] and the Three-Dimensional Rolling Contact Theory developed by Kalker [8,9]. These theories are based on the assumption of purely elastic behaviour and only work well for normal wheel tread-rail head contacts. As for measuring techniques, an electrical resistance method was presented by Bowden and Tabor [10] for real contact measurement, achieved by detecting the amount of electrical energy transmitted between the two bodies in contact. The main disadvantage of the method is that only the contact area is obtained, and the results are significantly affected by oxide layers on the component surfaces. A photo-elasticity technique characterises contacts based on the double refractive properties of some materials when they are pressed together [11]. The limitation of this method arises because most engineering components are made of metals, which do not have double refractive properties. There has been previous work measuring the contact stresses between two gear teeth where the components were made of photo-elastic materials, but the measurements made this way are inaccurate in not properly representing the real problem. Air flow is also used as a measuring tool for wheel-rail contacts [12]. Low pressure air is blown through a row of holes drilled on the rail top, air flow which is blocked, leading to an increase of air pressure, when the wheel passes over the holes on the rail. However, it is not practical to drill holes on in-service rail tracks and the results are of low resolution in any case due to the physical sizes and placing of the holes. Pressure sensitive film is commonly used for quick and straightforward contact information [13]. The film has a certain thickness, however, (around 0.5mm) and contact conditions can be severely altered by the film itself. Even then, pressure sensitive film has an upper contact stress detection limit of 300MPa, which is far lower than normal wheel-rail contact stresses.

The above measuring techniques are basically limited because of insufficient contact information and the techniques themselves alter the true contact condition being studied. The Finite Element Method (FEM) has been widely applied for wheel-rail contact simulations in recent years with the development of computing capability [14]. Yet the complexity of wheel/rail profiles and difficulties in simulating surface roughness, which is dominantly important for contact behaviours, limit the application of FEM to be more as a validation approach. Ultrasonic reflectometry, however, has proved useful for machine-element contact measurements [15] and particularly for static wheel-rail contact determination [16,17]. A high-resolution characterisation technique for wheel-rail contacts using a 64-element ultrasonic array has been developed in previous work by the authors [17,18]. Yet unlike conventional ultrasonic methods for defect detection, where defects can be indirectly inferred through inspection data or can be reached easily with guided waves, characterisation of contacts needs ultrasound beams striking precisely at the contact interfaces, whereas for the longitudinal elastic body waves normally used in this scenario, structural modifications of contact bodies are usually essential for proper sensor displacement [18]. In most cases, such modifications are strictly forbidden in railway engineering and hence limit the applicability of the technique. Facing this concern, in this paper, a truly non-invasive pitch-catch ultrasonic array sensing technique is proposed for characterising real-time dynamic wheel-rail contact, where relatively abundant contact information can be obtained without any pre-machining or modification to the rail structure. This is promising for use in a real-time monitoring of in-service HSR lines.

2. Principle of Ultrasonic Reflectometry

The surface of an engineering component is never perfectly flat or smooth no matter how well machined and finished. Distributed over the surface are tiny pinnacles known as asperities. When two machine elements are pressed together, it is only the asperities on the two surfaces which are in contact with each other. Ultrasonic reflectometry is based on the phenomenon that an ultrasound beam striking a contact interface will only be partially transmitted or reflected. The portion reflected is determined by the acoustic properties of the material the propagating the ultrasound and that of the material receiving it. The reflection coefficient, *R,* defined as the ratio of amplitude of the reflected signal and that of the incident signal, has a following relationship with the material properties of the contact bodies:

$$R = \frac{z_1 - z_2}{z_1 + z_2} \tag{1}$$

$$z = \rho c \tag{2}$$

where z_1 and z_2 are the acoustic impedances of the two materials in contact. ρ is material density and c is the speed of sound transmission through the material. As shown in Figure 1(a), when a beam of ultrasonic signal propagates in two materials with the same or similar acoustic impedances, say, steel-steel contacts, signals at the interface will be fully transmitted, whilst signals at the steel-air interface will be mostly reflected.

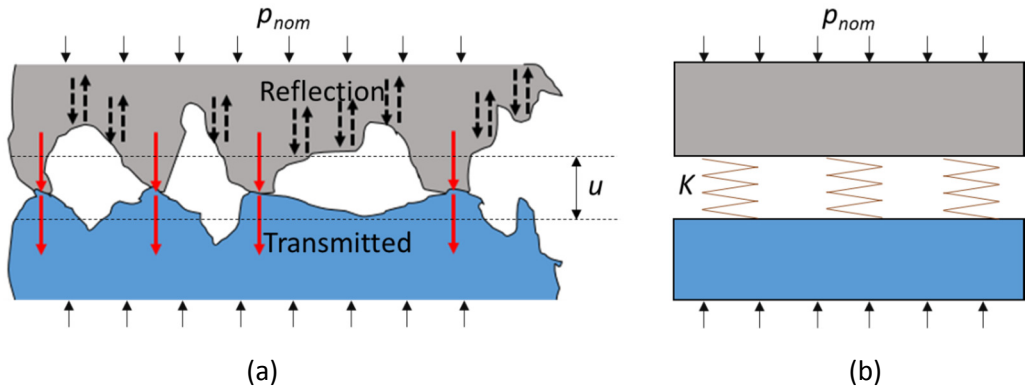

(a) (b)

Figure 1. Ultrasound behaviour at contact interfaces

Kendall and Tabor discovered that if the wavelength of ultrasound is relatively long in relation to the air gaps, the contact interface behaviour can be modelled as a spring [19] (Figure 1(b)). The interfacial stiffness, *K,* of the *spring* model was defined by Thomas & Sayles [20] as the differential of the nominal contact pressure with average distance between the mean positions of the two contacting surfaces.

$$K = -\frac{dp_{nom}}{du} \tag{3}$$

where *u* is the mean separation between the two surfaces in contact. When the two bodies are just slightly pressed together and barely any external load is applied, the interfacial stiffness *K* is close to zero indicating the asperities of the two contacting surfaces are either

in an initial contact state or completely not in contact. As the bodies are further compressed together with increasing load, more and more asperities are pressed into contact, leaving fewer and fewer air gaps and extra force is increasingly required to achieve further compression. Thus, *K increases* to infinity at the point when the bodies are in complete overall contact and no further spaces are left. In the case where the wavelength of the ultrasonic wave is relatively longer than the air gaps, increases in interfacial stiffness will cause growing amount of transmitted ultrasonic waves and lead to a reduction in the reflection coefficient.

The relationship between interfacial stiffness and reflection coefficient was quantified with the *spring* model further investigated by Drinkwater et al. [21]. For ultrasonic signals reflected from a rough contact interface, the magnitude of the reflection coefficient, *R,* has the following relationship with *K* (GPa μ/m):

$$|R| = \frac{\sqrt{(\omega z_1 z_2)^2 + K^2(z_1 - z_2)^2}}{\sqrt{(\omega z_1 z_2)^2 + K^2(z_1 + z_2)^2}} \tag{4}$$

where ω is the angular frequency of the wave ($\omega = 2\pi f$) and z_1 and z_2 are the acoustic impedances of the two contacting bodies. In the case of two bodies made of materials with the same acoustic properties, $z_1 = z_2 = z$, Equation 4 can be simplified to:

$$|R| = \frac{1}{\sqrt{1 + (2K/\omega z)^2}} \tag{5}$$

Although wheel and rail are different types of steel, their acoustic impedances are roughly be regarded as identical with similar densities and speeds of sound transmission. In this study, therefore, Equation 5 has been mainly used to derive interfacial stiffnesses from measured reflected ultrasonic signal values.

3. The Pitch-Catch Ultrasonic Measuring Technique

Previous work has successfully shown the capability of ultrasonic reflectometry in wheel-rail contact characterisation. Normally this is done with a pulse-echo configuration, i.e., an ultrasonic transducer is used as both a pulser and a receiver, and the propagating pathways of incident signals and reflected signals are along the same line but in opposite directions. Apart from static wheel-rail contact tests [15], a dynamic wheel-rail contact measuring approach is also proposed in previous work, based on a pulse-echo configuration, whereby an ultrasonic array is placed in a pre-machined T-slot situated at the rail web [16]. However, this approach requires modification to the rail structure which is not allowable on an in-service rail line. A new measuring approach is proposed here, therefore, which requires no modification to the rail. As shown in Figure 2, two sets of 10MHz piezoelectric sensors were installed on both sides at the bottom surface of the rail head. Each set consist of 8 linearly distributed ultrasonic elements made of Lead Zirconate Titanate materials, each element 2mm wide and 10mm long with a fixed gap of 0.5mm between two neighbouring sensors. The sensors were bonded onto the rail surface with a special “Tribobond” which has been developed by Tribosonics Ltd. and has an excellent ultrasound coupling effect, and the long

side of the sensors were oriented parallel to the longitudinal direction of the rail. Sensors on one side of the rail serve as pulsers, and sensors on the other side serve as receivers. When in operation, ultrasonic signals emitted from the pulsers are reflected at the rail top surface and captured by the receivers. This pitch-catch ultrasonic measuring technique provides a way to reveal contact information at the rail head. The pulsers are labelled 1 to 8 as shown in Figure 2 from inner bound to outer bound, and the receivers are correspondingly labelled A to H.

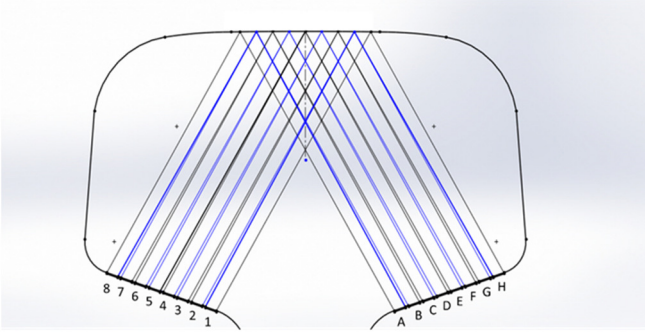

Figure 2. The pitch-catch ultrasound measuring technique

It should be noted that the ultrasonic signals are propagating in a conical pattern, i.e., with a growing area of wavefronts, rather than focussed straight lines, which leads to the fact that a signal emitted from one pulser can theoretically be detected by all the receivers, and vice versa. Figure 3 shows an example of A-scans measured from the two pitch-catch couples (PCCs) 4-B and 4-A. The reflected signals (marked in circles) can be clearly seen. The primary target of the authors' study was to investigate the optimum set of PCCs with most ultrasound energy and widest scanning range. By using ray-tracing software, the optimum set of PCCs was found to be 1-H, 2-G, 3-F, 4-E, 5-D, 6-C, 7-B, 8-A with signal directions almost perpendicular to the ultrasonic elements. Other sets of PCCs, however, can also provide useful information and is included in future work.

Figure 3. A-scans of different PCCs

As seen in Figure 3, for some PCCs, multi-reflections are observed. A series of tests have been carried out, which revealed that the second reflection derives from the signal reflected first from the rail head and then from the rail gauge corner. This phenomenon provides the possibility of monitoring wheel flange-rail gauge corner contacts and will be further investigated and reported in a separate paper. The study reported in this paper focusses on the first reflection and wheel tread-rail head contacts.

As shown in Figure 4, when in test, the first reflected signal of each PCC was 'zoomed in' for data extraction purposes, and the peak to peak values for all eight reflected signals were recorded for further processing.

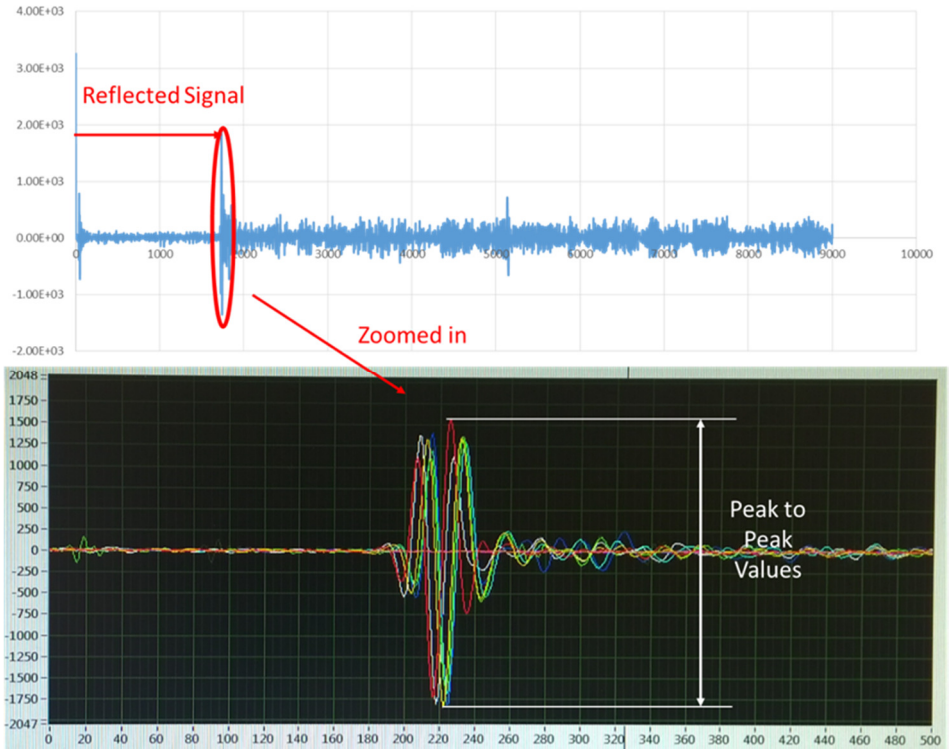

Figure 4. Data acquisition of first reflected signals

4. Scanning Range Investigation of Pitch-Catch Ultrasonic Sensors

Before the technique was applied to wheel-rail contact monitoring, a pilot study on the scanning range of each PCC was helpful. Ideally, we want the scanning range shown in Figure 3 to cover the entire rail head contact, with no gaps or overlaps. In practice, however, each pulser-receiver combination scanned a slightly larger area. To test to which part of the rail head a specific couple applied, as shown in Figure 5, a 32mm long paper ruler was attached to the rail head, with 16 divisions along the lateral direction, each 2mm wide, and a 2mm wide and 20mm long (long enough to cover the scanning range of the transducers in the longitudinal direction) rubber strip was made for pilot study. The rubber strip was moved 2mm laterally in a stepwise manner to align with every division of the paper ruler and was held against the rail surface by a metal block to provide even loading. When the rubber strip was compressed, the width grew by up to 4mm due to the high Poisson's Ratio of rubber,

and this further increased the number of influenced PCCs in one measurement. A reference measurement was taken without the rubber, and reflection coefficients plotted. For clarification, each PCC is displayed in a row, resulting in a 2-dimensional reflection coefficient map shown in Figure 6. The x-axis represents lateral positions of the rubber strip, and the y-axis represents the PCC. The reflection coefficients were plotted in a hot colourmap from white to dark red corresponding to the scale from 0 to 1. Lower reflection coefficients indicate greater degrees of contact.

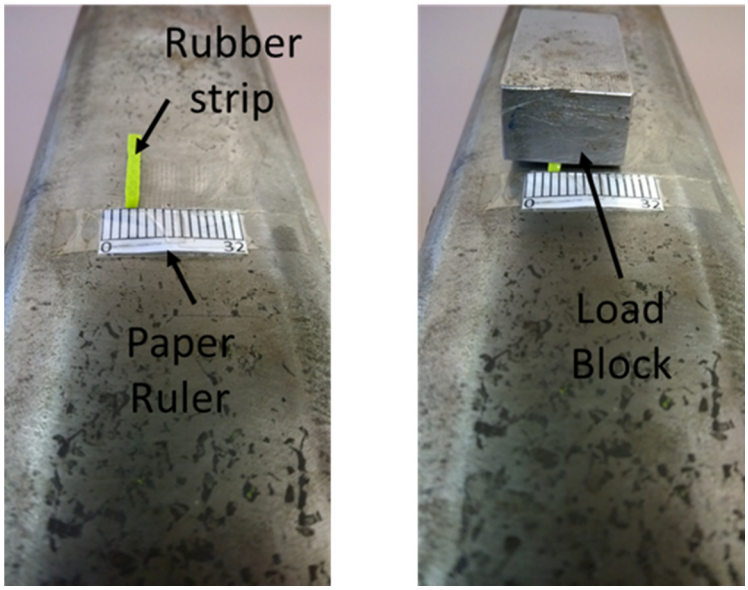

Figure 5. Scanning range test

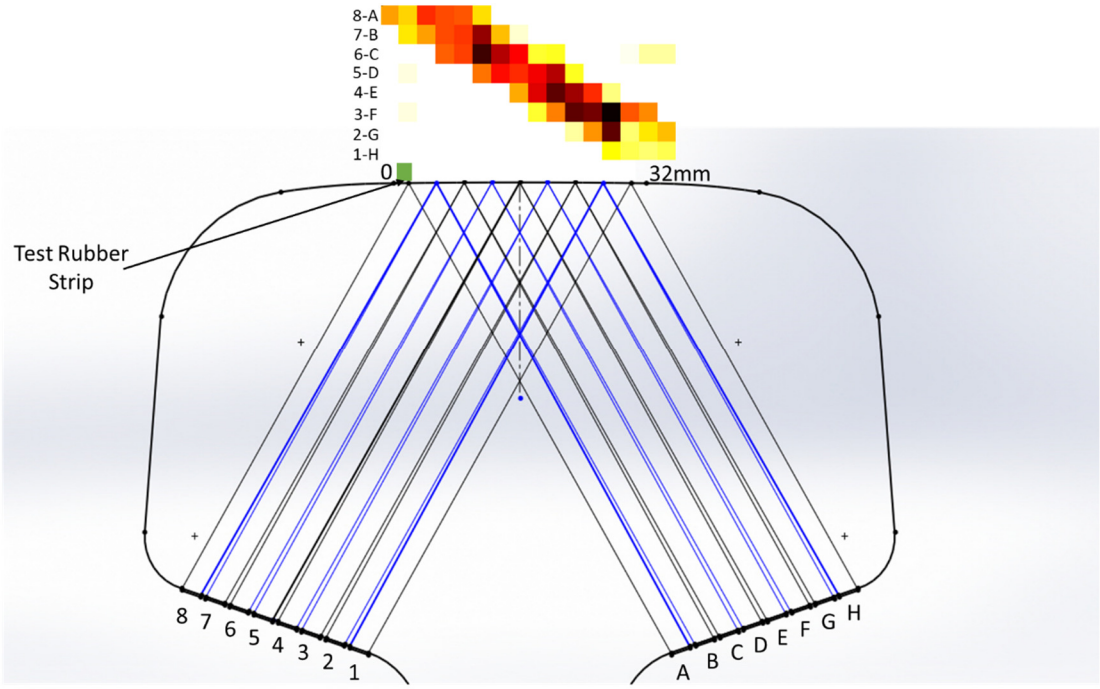

Figure 6. Reflection coefficient map of rubber at different lateral positions

From Equation 5 it can be concluded that lower reflection coefficient corresponds to higher interfacial stiffness, and consequently indicates higher contact stress. Figure 6 indicates that each PCC can be influenced by the contact interface up to 12-14mm along the lateral direction but is most sensitive to the middle point (4mm) of the potential scanning area, which means although the entire rail head is basically covered, there are information overlaps between neighbouring PCCs. However, for rough contact area estimation purpose, the 32mm railhead can be equally divided by the 8 PCCs. The test showed that the PCCs 8-A to 1-H scanned from left to right in order as expected and proved the capability of the technique in contact characterisation. The test also indicates that reflected signals from PCCs contain information of slightly larger contact areas than expectations.

5. Quasi-dynamic wheel-rail contact measurements

With the technique proved in the pilot study, a series of quasi-dynamic wheel-rail contact measuring tests were carried out. The test rig is shown in Figure 7, a wheel specimen cut from a full-scale train wheel was used in contact with a section of rail. The wheel specimen is 75mm long in the rolling direction, and the rail section is 300mm long. The wheel and rail test specimens were placed in a hydraulic-powered loading rig. The wheel specimen was fixed onto the upper part of the loading rig with a bolted joint, and the rail was slightly slanted with a thin steel plate inserted at the bottom of the rail foot to guarantee a wheel tread-rail head contact. The eight sensors on each side were integrated into a pulser array and a receiver array respectively. The two arrays were mounted using magnetic clamps to provide firm contact with the rail surface. When testing, the wheel was lowered down to make contact with the rail and then loaded through the hydraulic loading rig. The two arrays were linked to an FMS100 PC developed by Tribosonics Ltd. The FMS100 PC is a special type of desk with integrated multichannel ultrasonic pulsing and receiving (UPR) units as well as real-time data displaying and storage functions, and can operate through 8 channels simultaneously for ultrasonic testing and measurements.

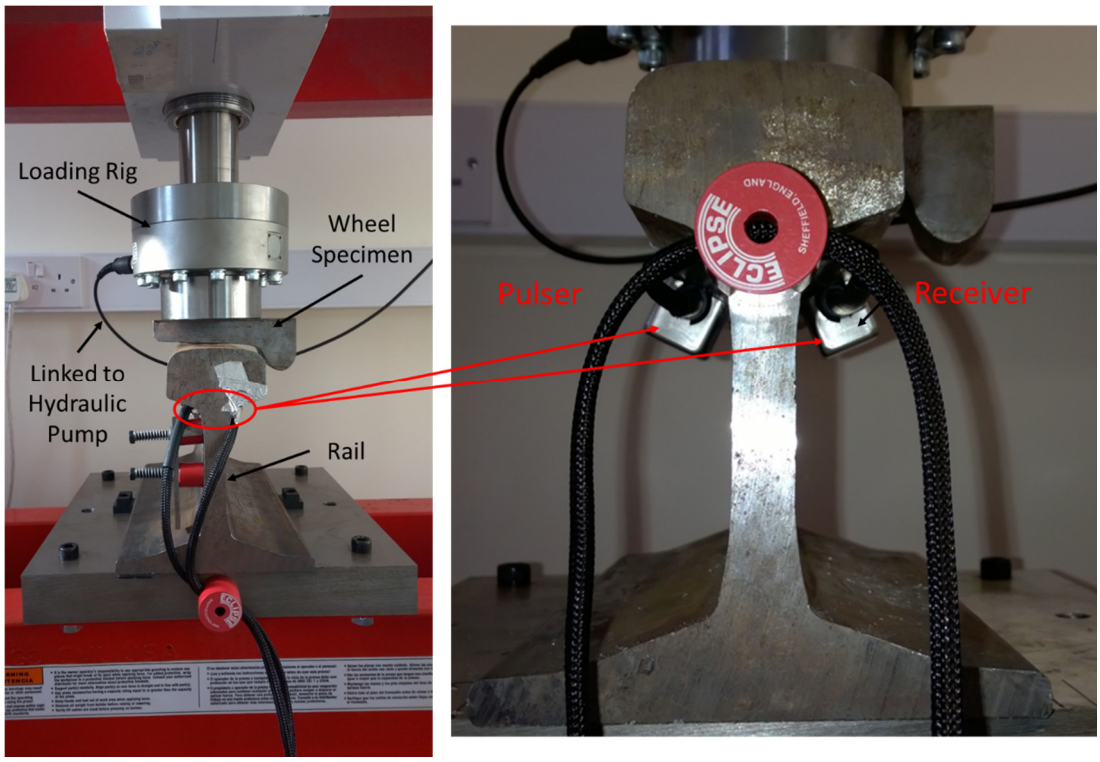

Figure 7. Test set-up of quasi-dynamic wheel-rail contact measurement

5.1 Static wheel-rail contact position monitoring test

The rail was moved laterally according to three positions marked on the support base as: centre, 15mm to the left (noted as -15mm) and 15mm to the right (noted as +15mm). It should be noted that due to the complexities of wheel and rail profiles, a lateral rail displacement does not mean an equal displacement of the contact patch, and for some cases a lateral movement of the rail could lead to the contact patch moving in the opposite direction. To validate the contact positions measured from ultrasonic reflectometry, blue paint was applied to the wheel. A 20kN load was applied at the wheel-rail contact patch, at the three rail positions, and for each position a contact patch was stamped on the rail head, as shown in Figure 8.

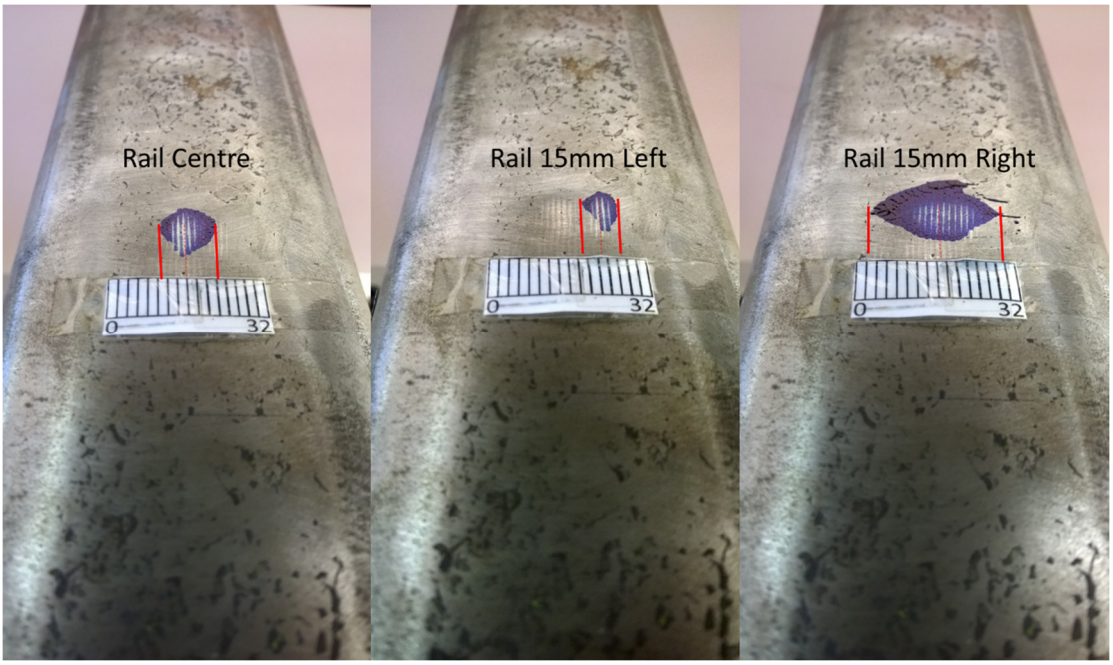

Figure 8. Wheel-rail contact patches when the rail is in centre, -15mm and +15mm positions

The blue stamp clearly marks the contact patch positions on the rail. The contact patch was in a central position for rail centre case, and the contact shape is a relatively regular ellipse; At the -15mm rail position, the contact patch moved about 7mm to the right, with a narrower contact shape; At the +15mm rail position, contact was more conforming with a larger contact patch. The widths (along lateral direction) of the contact patches were 11, 8 and 28 mm, respectively.

As for the ultrasonic pitch-catch tests, a series of loads ranging from 2kN to 20kN was applied, and a line of measurements was taken at each rail position under each load. The corresponding reflection coefficient lines indicating cross-sections of contact areas were plotted, as shown in Figure 9. A lower reflection coefficient indicates a further contact and a higher contact stress.

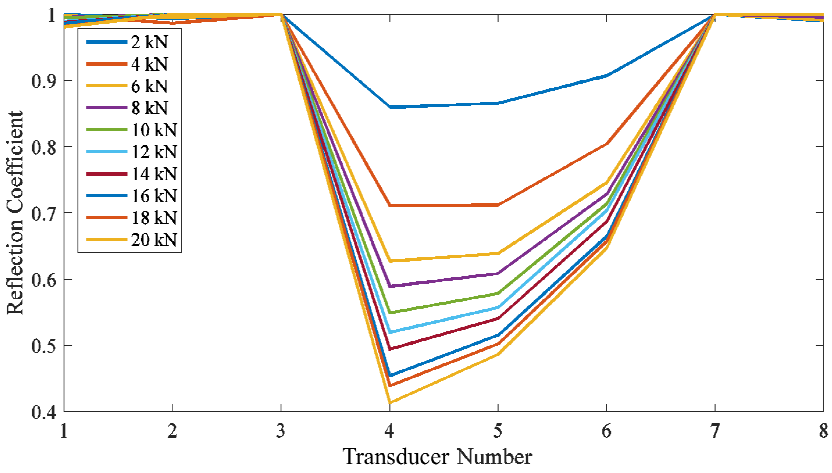

(a) Rail in centre position

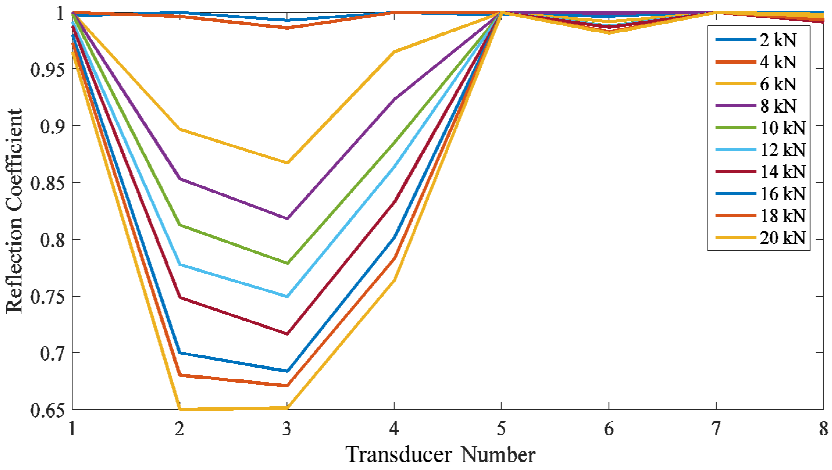

(b) Rail in -15mm position

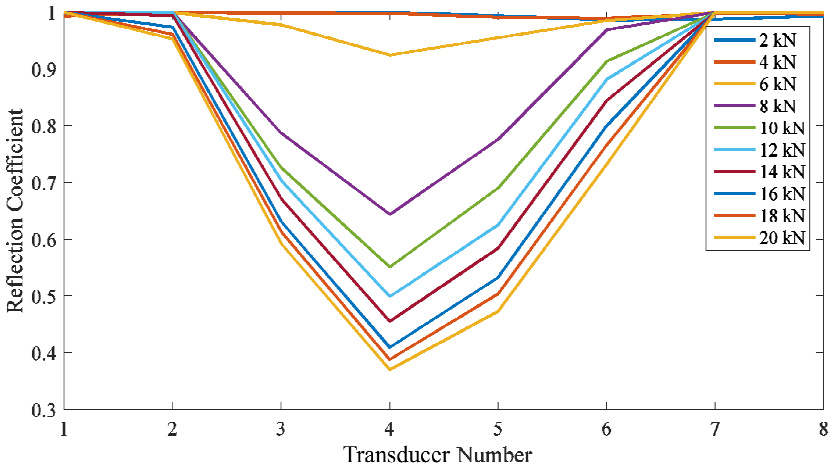

(c) Rail in +15mm position

Figure 9. Cross-sections of reflection coefficient of wheel-rail contacts with different rail positions

Figure 9 shows that the reflection coefficients acquired from the pitch-catch ultrasonic technique decrease with increasing load. The transducer number aligns with the pulser labels. It should be noted that pulsers 1-4 scan the right-hand side of the rail head and pulsers 5-8, the left. Therefore, the contact positions measured in Figure 9 are mirrored as those shown in Figure 8. Although scan range overlaps exist between neighbouring PCCs, as indicated in Section 4, by assuming each PCC covers a 4mm scanning range, the widths of the contact patches can be roughly approximated as: 16mm, 16mm and 28mm respectively. Due to the resolution limitation and the low loads applied, the growth in contact size with increasing load is not obviously seen in Figure 9. However, the capability of the method to capture sufficient wheel-rail contact information has been demonstrated.

5.2 Quasi-dynamic test

The quasi-dynamic test was carried out subsequently by manually moving the rail longitudinally to simulate dynamic wheel-rail contact. A line of measurements was taken at every 1mm movement of the rail n the longitudinal direction. A 60kN load was applied, and for the 12 rail positions measured, a 2-D reflection hot colourmap was plotted in Figure10, showing the contact patch.

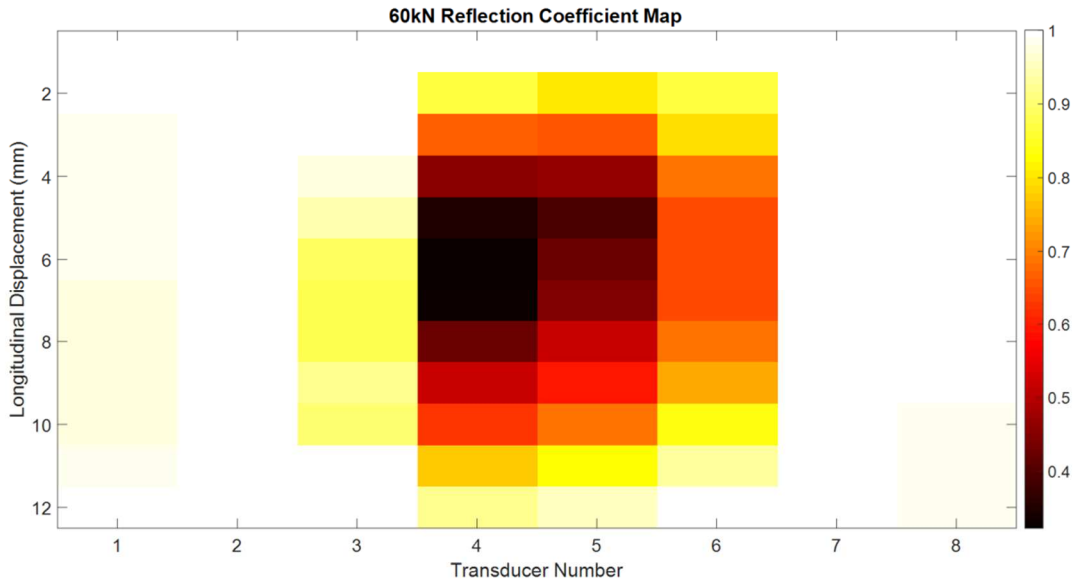

Figure 10. Reflection coefficient map of quasi-dynamic wheel-rail contact

In Figure 10, although resolution is limited, the contact patches can be readily seen. The figure shows a gradual stress growth from rail edge to centre. Ellipses could be roughly drawn demonstrating the contact zone.

6. Full-Scale Dynamic Wheel-Rail Contact Characterisation

6. 1 Full-scale dynamic test set-up and results

With all the pilot work accomplished, a full-scale dynamic wheel-rail test was carried out. The test was done on a full-scale wheel-rail test rig as shown in Figure 11, on which the rail can be pulled back and forth at a controlled speed with an actuator, and the wheel is fixed in the longitudinal direction and is allowed to rotate freely. In this way, the behaviour of a wheel rolling on a rail can be simulated.

Figure 11. Full-scale wheel-rail test rig

A schematic of the testing arrangement is shown in Figure 12. The pitch-catch arrays were installed on both sides of the rail and connected to a PC via a Junction Box for easy wire ordering. The rail is 1200mm long and the maximum moving distance is 400mm. For the dynamic tests of this study, the test length was 200mm which is enough to capture a complete contact patch. A 1 to 20 wedge was used for rail inclination to guarantee a full wheel tread-rail head contact. Rail inclination is also important and widely applied in real railway lines to sustain good wheel-rail contact conditions. Limited by the pulsing rate from current hardware and test rig, the test speeds were 5mm/s and 20mm/s. For each speed, loads from 40kN to 120kN were applied.

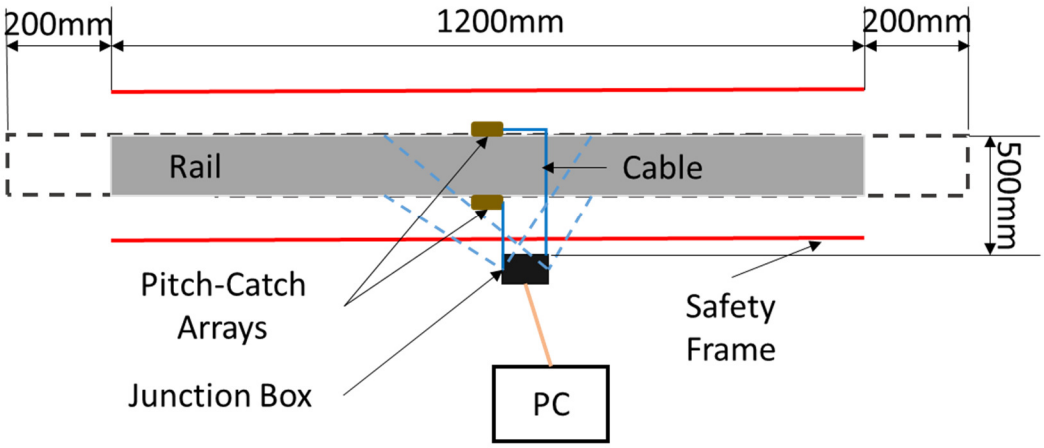

Figure 12. Full-scale dynamic wheel-rail contact measurement set-up

To start the test, the wheel was lowered until fully supported by the rail. The rail was then actuated to provide a longitudinal movement. The pitch and catch arrays took continuous measurements up to the maximum rail movement range of 200mm. The wheel was then lifted, and the rail was pulled back ready for the start of the next cycle. Wheel/rail not-in-contact measurements were taken as a reference to obtain the reflection coefficients which were calculated by dividing the measurements taken in loading conditions with reference data in unloaded case. Subsequently, rewriting Equation 5 as:

$$K = \frac{\omega z}{2}\sqrt{\frac{1}{|R|^2} - 1} \tag{6}$$

the interfacial stiffness map can be obtained from Equation 6, and a relationship between *K* and contact pressure *P* for a certain surface roughness pair can be found with a calibration experiment taken. The calibration specimens were machined from the same material and to the same surface finish as the wheel and rail test components. Marshall et al. investigated three different wheel-rail surface finishes: un-used, sand-damaged and worn tread. Corresponding *K*-*P* relationships which are approximately linear over the tested pressure range were obtained. The wheel and rail of the dynamic test were worn, both wheel tread and rail head, and the *K*-*P* relationship according to [16] would be $P = 123K$. Eventually pressure maps are plotted as shown in Figure 13.

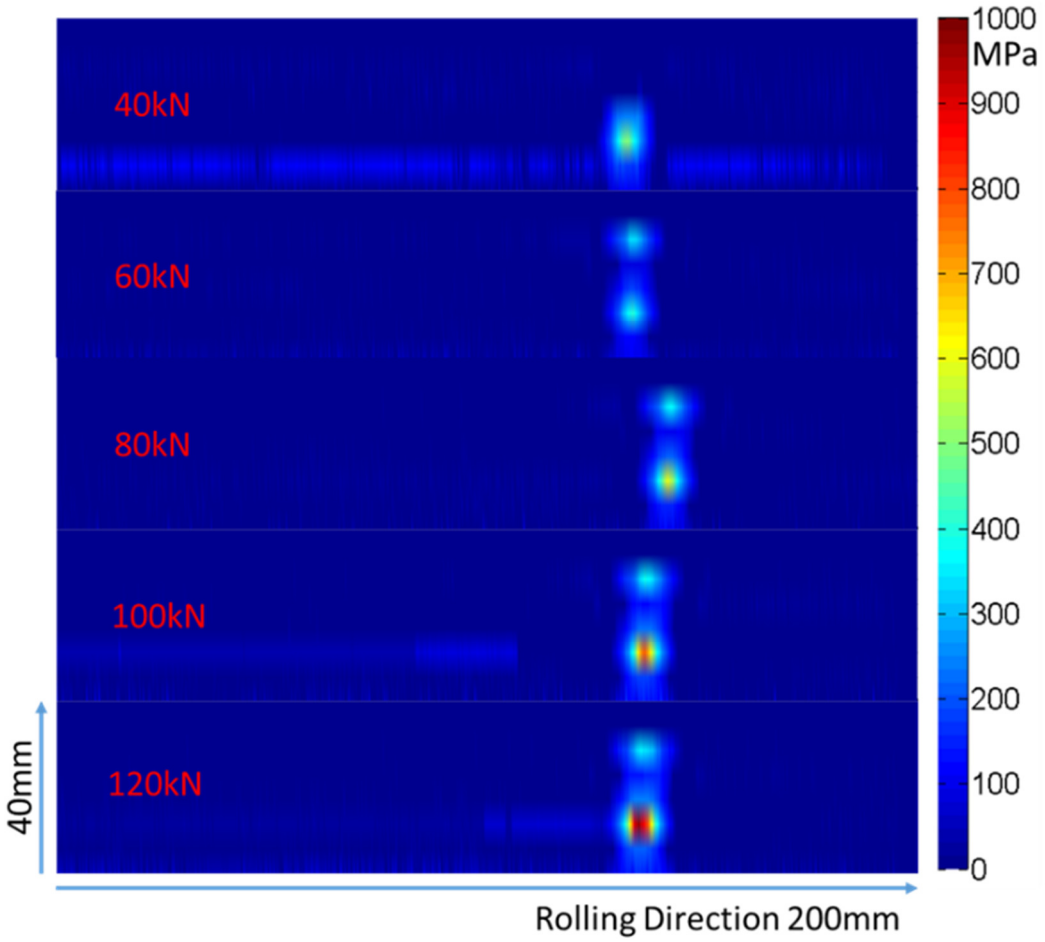

(a) 5mm/s

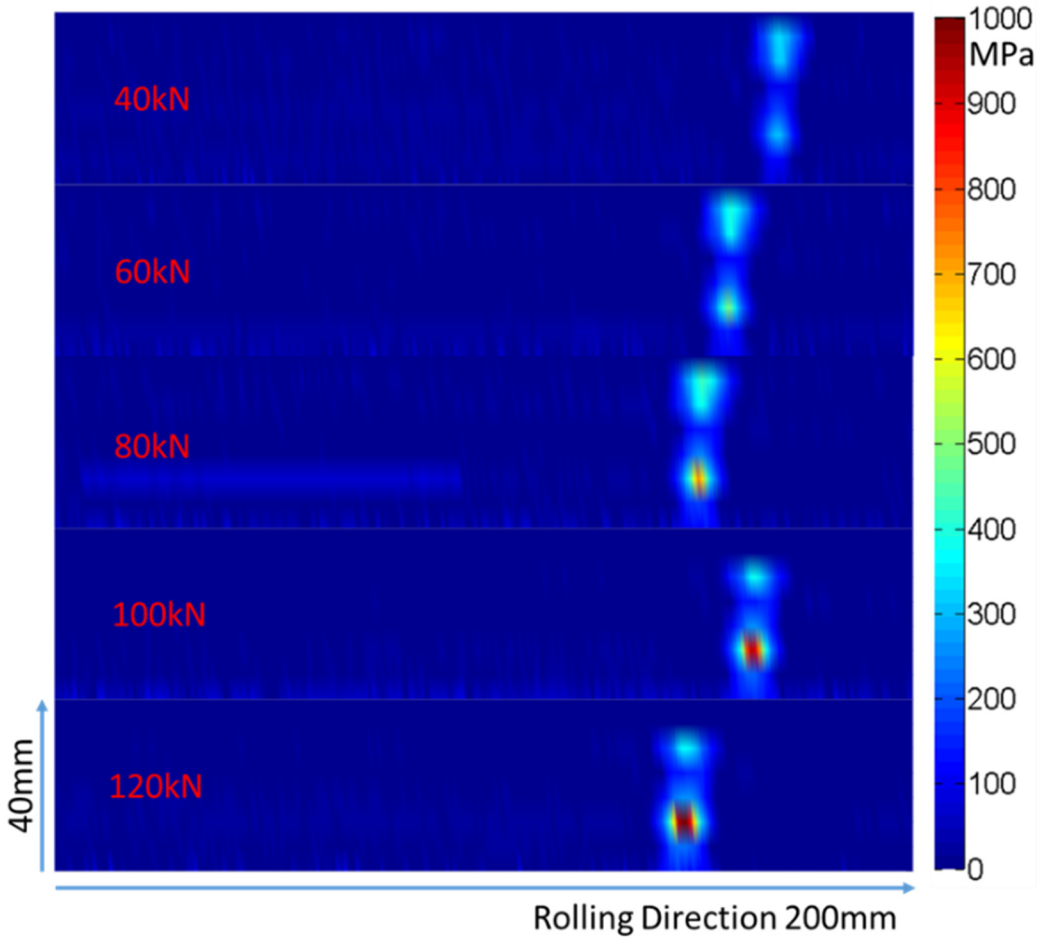

(b) 20mm/s

Figure 13. Contact pressure distribution of dynamic wheel-rail contact with different loads and different speeds

Contact patches can be clearly viewed in the pressure distribution map of Figure 13, and a double-contact patch was captured. Since the wheel tread and rail head were both worn, more than one wheel-rail contact tends to be more conformal leading to more than one contact points, which were successfully detected in the test. With increasing loads, the measured contact pressure and contact size grew accordingly. The peak contact pressure under different loads were 395, 496, 584, 765, 972MPa for the 5mm/s test and 330, 478, 720, 926, 998MPa for 20mm/s respectively. Although the test speed in the lab environment was low, the test results are stable under different speeds and the outlook is promising, that high quality contact information can be expected from high speed field tests.

For validation purposes, a static wheel-rail contact test was carried out using a section of wheel and rail having the same surface finish as the wheel and rail of the dynamic test. As shown in Figure 14, the wheel and rail sections were pressed together in a loading rig by hydraulic pump. An ultrasonic transducer was used to scan the top of the loading rig, and the scanning window was filled with distilled water couplant so that ultrasound signals could be focused at the wheel-rail interface. An ultrasonic pulser and receiver (UPR) for generating and receiving ultrasound signal was connected to a PC and an oscilloscope. The transducer

can move in the horizontal plane to acquire a two-dimensional measurements scan. Measurements were taken under the loads 40kN, 60kN and 80kN respectively, sufficient for validation purposes.

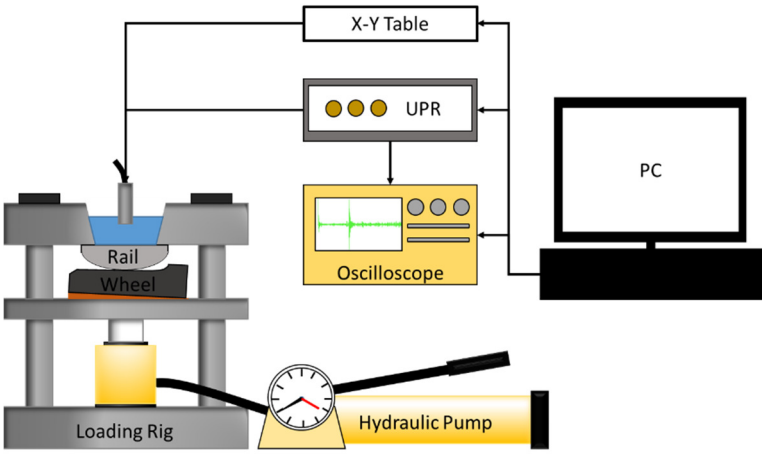

Figure 14. Test setup of static wheel-rail experiment

As above in Section 4, contact area can be roughly estimated regarding each PCC corresponds to the most sensitive 4mm, but each measurement taken literally relates to a pressure average on the contact area of 12-14mm laterally. Resolution in the longitudinal direction is determined by the rolling speed of the wheel and the pulse repetition frequencies (PRF) of the ultrasound excitation equipment. In the static test, however, the resolution is determined by the size of the focusing point (which is determined by the frequency of the ultrasonic probe and slightly varies subject to manufacturers, the diameter of the focusing point of the 10MHz probe used in the study is 0.9mm) of the ultrasonic probe and the step length of the scanning tank (0.5mm), leading to a pressure map with much more details, as shown in Figure 15. The static measurements, therefore, are more likely to capture the high stress concentrations of the asperity contacts, resulting in much higher peak contact pressure measurements.

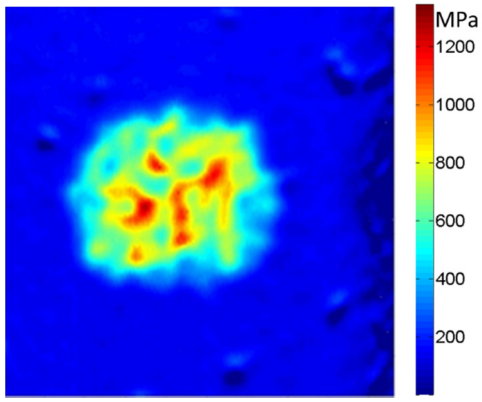

Figure 15. Wheel-rail contact pressure map from static test under 80kN

In recognition of this, results from the static test and Hertz theoretical predictions were averaged over a 4mm circular neighbourhood around the peak pressure point (as a

representative example), in a same manner as a dynamic measurement is obtained, to compare and validate the pressure characterising capability of the proposed dynamic method. The Hertzian pressures were calculated by using profile parameters and material properties (lateral and longitudinal radius and Young's modulus) of the tested wheel and rail specimens.

Load (kN) / Method	40	60	80
Hertz	443 (649)	582 (842)	710 (972)
Static	402 (850)	562 (1029)	708 (1242)
Dynamic 5mm/s	395	496	684
Dynamic 20mm/s	330	478	720

Table 1. Averaged-peak contact pressure (MPa) comparison (numbers in the bracket are the peak pressures before averaging)

6.2 Discussion

The comparison shows a promising consistency in terms of the averaged-peak contact pressures among dynamic results under two speeds, static results and Hertz predictions. This validates well the pitch-catch method for contact characterisation. It is worth noting that that although the comparisons show that proposed method provides roughly correct contact pressure levels of the contact of interest, but does not indicate the absolute accuracy in pressure determination, even though the numbers in Table 1 are close to each other. Although a series of measures were taken to make contact conditions similar (type and surface finish of wheel and rail specimens), significant variances are still inevitable. A most obvious difference is that single contact patches were captured in static tests, consistent with Hertz assumptions, but in dynamic tests, multiple contact patches were observed due to increased surface conformal contact caused by wear of the tested wheel and rail.

From another perspective, the ability to detect multiple contact patches by the pitch-catch method is satisfactory since a large number of multi-contacts occur in real in-service rail systems [22].

To enable practical applications of the technique on real operating rail lines, future work has already been thoroughly planned to improve both performance and applicability.

One major refinement is the ability to take measurements under wheels running at high speeds. This ability, as illustrated above, is determined by the PRF of the ultrasound excitation device. In the study reported in this paper, the concept was well proven at very low speeds (5mm/s and 20mm/s) with a restricted PRF (10 Hz) with the currently available equipment. Hardware and system upgrades are in progress, and it is expected to be able to characterize dynamic wheel-rail contacts at in-service running speeds when this is completed. Figure 16 shows the number of measuring points needed for different PRFs and vehicle speeds.

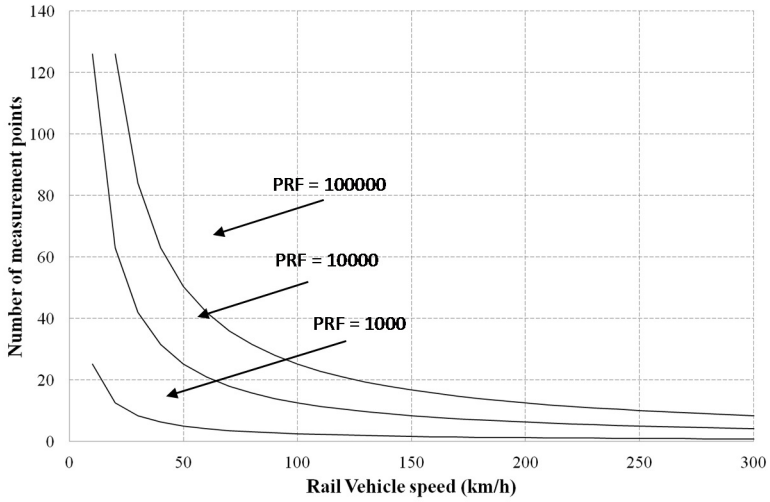

Figure 16. The number of measurements as the rail vehicle passes over the array transducer as a function of pulse repetition frequency [17].

As clearly demonstrated in the present work, contact information can be adequately revealed by as few as 8 measurements. From Figure 16 it can be concluded that when the PRF reaches 1000Hz, the technique is useful for vehicle speeds of around 50km/h. For a PRF of 100000Hz, the technique can measure contact at 250km/h, which is the operating speed of high-speed trains.

Another improvement is in lateral resolution. Since the space under the rail head is limited, whilst a minimum size of the PZT elements has to be guaranteed for normal functioning, it would be helpful if more information could be interpreted from less sensors deployed. As above in Section 3, responses can be seen from all possible PCCs, though not made use of in the study of this paper. Hereby same notations of all pulsers and receivers in Section 3 are inherited and the mid-point of the scanning range of each PCC is taken as indicating reference. By dividing the whole scanning range into 15 isometric sub-areas, the PCCs and corresponding sub-areas can be easily linked together as in Table 2. Each colour represents a set of PCC relating to various combinations of from pulser 1 to 8 and receiver A to H. The underlined letters in italic font are the combinations used in previous tests. As stated, the measurements in present work are literally pickups in an interlacing way from the complete table of measurement. For example, the resolution used in this study can be instantly doubled by carrying out further tests with the combination sets 7-A, 6-B, 5-C, 4-D, 3-E, 2-F, 1-G and 8-H.

Sub Area Number	1	2	3	4	5	6	7	8	9	10	11	12	13	14	15
pulser 8	A	B	C	D	E	F	G	H							
pulser 7		A	B	C	D	E	F	G	H						
pulser 6			A	B	C	D	E	F	G	H					
pulser 5				A	B	C	D	E	F	G	H				
pulser 4					A	B	C	D	E	F	G	H			
pulser 3						A	B	C	D	E	F	G	H		
pulser 2							A	B	C	D	E	F	G	H	
pulser 1								A	B	C	D	E	F	G	H
Lateral Position	2.5mm	5mm	7.5mm	10mm	12.5mm	15mm	17.5mm	20mm	22.5mm	25mm	27.5mm	30mm	32.5mm	35mm	37.5mm

Table 2. Scanning range of all PCCs

As it can be seen in Table 2, the centre point of the rail head is scanned by all 8 pulsers, and the number of influencing PCCs decreases as the zone of interest moves towards the sides of the rail head. Only one PCC scans the very left-hand sides of the rail head and only one scans the very right-hand side (8-A and 1-H, respectively). Thus the 2-D reflection coefficients and contact pressure distribution maps have high resolution properties at the rail centre and lower resolution at the sides along the lateral direction, as shown in Figure 17 (each colour indicates a fixed length).

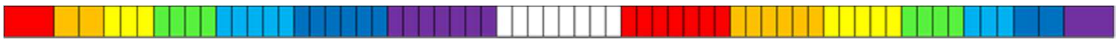

Figure 17. Schematic image of gradually changing resolution along lateral direction

Further thinking concerns the data deconvolution process by knowing the ultrasonic energy distribution function. A row of 64 measurements can be deconvoluted into 512 or even more points across the rail head to enable extremely high-resolution characterisation.

7. Conclusions

This paper introduces a new strategy for characterizing real-time dynamic wheel-rail contact using ultrasonic reflectometry. The approach utilizes a pitch-catch configuration taking advantage of the profile if the rail itself. Experimental investigations were made from the propagation pathway study of ultrasounds in a railhead, to scanning area of each PCC and validation of the concept via static and quasi dynamic tests. Full-scale dynamic wheel-rail tests were carried out next. Despite of the relatively low level of lateral resolution compared with previous related work by the authors due to data overlaps caused by ultrasound beam spreads at the reflecting interface and the limited space available for sensor deployment, the proposed technique provides sufficient information on wheel/rail interfacial contacts and demonstrates that the method is capable of the detection of multiple contact patches in situations of significant wear relating to real trains in service. Dynamic measurements showed good agreement with static test measurements and Hertz theoretical predictions in terms of general contact pressure levels. In contrast to previous work [17,18], the pitch-

catch strategy achieves a truly non-invasive method of monitoring wheel-rail contact conditions, and no modification to the to the rail structure is required. With relevant software and hardware upgraded, the new approach is expected to characterise and monitoring contacts between the instrumented rail track and all passing train wheels on operating high-speed lines.

Acknowledgements

The authors would like to appreciate the technical and equipment support by Tribosonics Ltd., UK.

References

[1] J. Peng, G.Y. Tian, L. Wang, Y. Zhang, K. Li, X. Gao (2015). "Investigation into eddy current pulsed thermography for rolling contact fatigue detection and characterization". *NDT & E International*, 74, 72-80.

[2] H.Y. Tam, T. Lee, S.L. Ho, T. Haber, T. Graver, A. Méndez (2007). "Utilization of fiber optic Bragg Grating sensing systems for health monitoring in railway applications". *Proceedings of the 6th International Workshop on Structural Health Monitoring*, 11th-13th September, Stanford, CA, USA.

[3] R.S. Edwards, A. Sophian, S. Dixon, G.Y. Tian, X. Jian (2006). "Dual EMAT and PEC non-contact probe: applications to defect testing". *NDT&E International*, 39, 45-52.

[4] P.W. Loveday (2012). "Guided wave inspection and monitoring of railway track". *Journal of Nondestructive Evaluation*, 31, 303-309.

[5] Y. Shen, C.S. Cesnik (2017). "Local Interaction Simulation Approach for Efficient Modeling of Linear and Nonlinear Ultrasonic Guided Wave Active Sensing of Complex Structures". *Journal of Nondestructive Evaluation*. 1(1), 011008-011008-9.

[6] M. Hong, Q. Wang, Z. Su, L. Cheng (2014). "*In situ* health monitoring for bogie systems of CRH380 train on Beijing–Shanghai high-speed railway". *Mechanical Systems and Signal Processing*, 45, 378-395.

[7] H. Hertz (1882). "Ueber die Berührung fester elastischer Körper". *Journal für die reine und angewandte Mathematik*, 1882(92), 156-171.

[8] J.J. Kalker (1990). "Three-Dimensional Elastic Bodies in Rolling Contact". Kluwer Academic Publishers, Dordrecht, Boston, London.

[9] J.J. Kalker (1982), "A Fast Algorithm for the Simplified Theory of Rolling Contact". *Vehicle System Dynamics*, 11(1), 1-13.

[10] F.P. Bowden, D. Tabor (1950). "The Friction and Lubrication of Solids", Clarenden Press, Oxford.

[11] H. Fesseler, E. Ollerton (1957). “Contact Stresses in Toroids Under Radial Loads”. *British Journal of Applied Physics*, 8(10), 387-394.

[12] W. Poole (1987). “The measurement of contact area between opaque objects under static and dynamic rolling conditions”. *Proceedings of Contact Mechanics and Wear of the Wheel/rail System*, University of Rhode Island, Waterlooville Press, 59-72.

[13] M. Pau, F. Aymerich, F. Ginesu (2001). “Measurements of nominal contact area in metallic surfaces: a comparison between an ultrasonic method and a pressure sensitive film”. *Wear*, 249, 533-535.

[14] X. Zhao, Z. Li (2011). “The solution of frictional wheel–rail rolling contact with a 3D transient finite element model: Validation and error analysis”. *Wear*, 271, 444-452.

[15] M.B. Marshall, R. Lewis, R.S. Dwyer-Joyce (2006). “Characterisation of Contact Pressure Distribution in Bolted Joints”. *Strain*, 42(1), 31-43.

[16] M.B. Marhsall, R. Lewis, R.S. Dwyer-Joyce, U. Olofsson, S. Bjorklund (2004). “Ultrasonic characterisation of a wheel/rail contact”. *Tribology Series*, 43, 151-158.

[17] H. P. Brunskill, A. Hunter, L. Zhou, D. J. Rob, R. Lewis (2018). “An Evaluation of Ultrasonic Arrays for the Static and Dynamic Measurement of Wheel Rail Contact Pressure and Area”. Submitted to *Proceedings of the Institution of Mechanical Engineers, Part J, Journal of Engineering Tribology*, (Ref. No. JET-18-0218).

[18] L. Zhou, H. P. Brunskill, R. Lewis, M. Pletz, W. Daves, S. Scheriau (2018). “Real time Measurement of Dynamic Wheel-Rail Contacts Using Ultrasonic Reflectometry”. Submitted to *Journal of Tribology*, (Ref. No. TRIB-18-1281).

[19] K. Kendall, D. Tabor (1971). "An Ultrasonic Study of the Area of Contact between Stationary and Sliding Surfaces", *Proceedings of the Royal Society, Series A*, 323(1554), 321-340.

[20] T.R. Thomas, R.S. Sayles (1977). "Stiffness of Machine Tool Joints: A Random-Process Approach". *Journal of Engineering for Industry*, 99(1), 250-256.

[21] B.W. Drinkwater, R.S. Dwyer-Joyce, P. Cawley (1996). "A Study of the Interaction between Ultrasound and a Partially Contacting Solid-Solid Interface", *Proceedings of the Royal Society Series A*, 452(1955), 2613-2628.

[22] J. Xu, P. Wang, L. Wang, R. Chen (2016). “Effects of profile wear on wheel-rail contact conditions and dynamic interaction of vehicle and turnout”. *Advances in Mechanical Engineering*, 8(1), 1-14.